Constitutive integration algorithms in metal warm forming

IOP Conf. Series: Materials Science and Engineering **493** (2019) 012013 doi:10.1088/1757-899X/493/1/012013

Constitutive integration algorithms in metal warm forming

D. Zhao [1, 2], W.Y. Zhao [1, 2], T. Jin [1, 2], H.Q. Fang [1, 2, *] and Z.H. Wang [1, 2]

[1] College of Mechanics, Institute of Applied Mechanics and Biomedical Engineering, Taiyuan University of Technology, Taiyuan, China
[2] Shanxi Key Laboratory of Material Strength and Structural Impact, Taiyuan University of Technology, Taiyuan, China

*Corresponding author e-mail: fanghuiqing@ tyut.edu.cn

Abstract. In this paper, two implicit integration algorithms are summarized in computational process, and an explicit numerical algorithm is presented for rate-dependent crystal plasticity in aluminium alloy warm forming, which is based on the forward Euler method. The plastic incompressibility and numerical accuracy are discussed in these algorithms. In this model, the plastic deformation gradient is chosen as controlling variable. The thermal deformation gradient representing the thermal history is introduced, and the plastic dissipation and the different temperature changing rates are considered in finite deformation computation. The expression of temperature dependent resolved stress is deduced form the thermodynamic framework. The mechanical behavior of Al polycrystalline in warm forming is computed and compared with different algorithms.

1. Introduction

Warm formed parts have been used in cars to reduce vehicle weight and improve safety. Deformation of the metal blank starts at higher temperature, and the different temperature changing rates also affect the deformation directly during the manufacturing process. In order to describe the deformation accurately, the constitutive relation of the metal should contain the thermal effects.

According to expression form of constitutive equation with thermal effects, which can be divided into two main categories. One is the constitutive equation given by stress function of strain, strain rate and temperature, which contains phenomenological and physical-based models. As a typical example of the phenomenological models, the Johnson-Cook model[1] presents the exponent form of strain and temperature to describe the stress flow, which is commonly used to simulate the deformation of metals and alloys in high strain rate and high temperature. Recently, Sung et al.[2] presented a new constitutive form describing the flow stress. The novel feature in their strain hardening function is twofold. Firstly, a linear combination coefficient was introduced to incorporate the Hollomon (power law form) and Voce (saturation behavior) model together. Secondly, the coefficient they introduced varies with temperature. In physical-based constitutive models, the thermal activation theory and dislocation dynamics are used to describe the mechanical response of the materials[3-6]. In these models, the activation energy for deformation dependent on temperature and dislocation-parameters, such as dislocation density, burgers vectors et al., are introduced into the flow stress functions. These constitutive models have simple computation forms, but the parameters for the models are complicated to be determined by the experiments.

Another category is based on the frame of crystal plasticity that using the thermal activation theory to describe the thermal effect. The activation energy depended on the temperature is used to describe the activation rates of dislocation[7-9]. Numerical algorithms of integration constitutive equations based on several primary integration variables, second P-K stress, shearing rate, plastic deformation gradient and elastic deformation gradient[10]. The implicit scheme was used to solve these equations to ensure the numerical stability. Ganapathysubramanian et al.[9] presented a fully implicit crystal constitutive algorithm considering small temperature changes and thermal activation of dislocations, which solved using a N-R approach with line search. Cry et al.[11] has presented a new single crystal thermo elasto-viscoplastic constitutive relation for aluminum alloy warm forming, and a new thermal slip-softening model is developed to control the thermal effect on slip rates. Zhao et al.[12] introduced the thermal part of velocity gradient into kinematics equation to reflect the thermal history, and an improved implicit integration algorithm with the plastic deformation gradient as the basic controlling variable is presented. But during the implicit computation, the Jacobian matrix should be updated in every iteration, and the formula deduction is complicated.

In this paper, an improved explicit integration model and two implicit algorithms are described to simulate thermo-elasto-viscoplastic deformation of crystals. The thermal deformation gradient representing the thermal history is introduced into the governing equation, and plastic dissipation and different temperature changing rates are analyzed in the finite deformation computation. The explicit computational process are compared with two implicit algorithms with elastic deformation gradient and plastic deformation gradient as the basic integration variable separately. The mechanical behavior of 1100Al in warm forming is computed using different integration algorithms, and the plastic incompressibility, different strain rates and numerical accuracy will be introduced next.

2. Kinematics

In order to include thermal effects, the intermediate thermal configuration, between the initial configuration and the deformed configuration, is introduced into the kinematics of a single crystal deformation. The total deformation gradient is decomposed into three parts as follows[12]

$$\mathbf{F} = \mathbf{F}^e\mathbf{F}^p\mathbf{F}^\theta \tag{1}$$

Where $\mathbf{F}^e$ is the elastic deformation gradient, $\mathbf{F}^p$ is the plastic deformation gradient and $\mathbf{F}^\theta$ is the thermal part of the deformation

gradient. Assuming isotropic thermal expansion, the thermal deformation gradient is given by

$$\mathbf{F}^\theta = [1+\beta(\theta-\theta_0)]\boldsymbol{\delta} \tag{2}$$

Where $\boldsymbol{\delta}$ is the second-order identity tensor, β is the thermal expansion coefficient, θ is the current temperature and θ_0 is the initial temperature. Using equation (1), the velocity gradient is expressed as

$$\mathbf{L} = \dot{\mathbf{F}}\mathbf{F}^{-1} = \mathbf{L}^e + \mathbf{F}^e\mathbf{L}^p\mathbf{F}^{e^{-1}} + \mathbf{F}^e\mathbf{F}^p\mathbf{L}^\theta\mathbf{F}^{p^{-1}}\mathbf{F}^{e^{-1}} \tag{3}$$

With

$$\mathbf{L}^e = \dot{\mathbf{F}}^e\mathbf{F}^{e^{-1}} \tag{4}$$

$$\mathbf{L}^\theta = \dot{\mathbf{F}}^\theta\mathbf{F}^{\theta^{-1}} \tag{5}$$

$$\mathbf{L}^p = \dot{\mathbf{F}}^p \mathbf{F}^{p^{-1}} = \sum_\alpha \dot{\gamma}^a \overline{\mathbf{P}}^\alpha \tag{6}$$

Where $\mathbf{L}^e$ is elastic velocity gradient, $\mathbf{L}^\theta$ is the thermal part of velocity gradient represents the evolution of the intermediate thermal configuration, $\mathbf{L}^p$ is the plastic velocity gradient relative to the relaxed configuration, which is defined using the rate of shearing on the αth slip system $\dot{\gamma}^a$ and the Schmid orientation tensor $\overline{\mathbf{p}}^\alpha$ .The Schmid orientation tensor in relaxed configuration is defined by the dyadic product of slip direction $\overline{\mathbf{s}}^\alpha$ with slip plane normal vector $\overline{\mathbf{m}}^\alpha$. FCC single crystal contains twelve {111} <110> slip systems.

3. Constitutive model

Elastic deformation is described by the second Piola-Kirchoff stress $\mathbf{T}$ and the Green strain tensor $\mathbf{E}$.

$$\mathbf{T} = \mathbf{C}(\theta) : \mathbf{E} \tag{7}$$

$$\mathbf{E} = \frac{\mathbf{1}}{\mathbf{2}}(\mathbf{F}^{\mathbf{eT}}\mathbf{F}^{\mathbf{e}} - \mathbf{I}) \tag{8}$$

Where, $\mathbf{C}(\theta)$ is fourth-order anisotropic elasticity tensor dependent on temperature.

The shearing rate on each slip system $\dot{\gamma}^\alpha$ and its corresponding resolved shear stress τ^α are used to describe the plastic deformation. The shearing deformation rate dependent on temperature adopts the following form[13]

$$\dot{\gamma}^\alpha = \dot{\gamma}_0 \left| \frac{\tau^\alpha(\theta)}{\hat{\tau}^\alpha(\theta)} \right|^{\frac{1}{m}} sign(\tau^\alpha) \tag{9}$$

Where, $\hat{\tau}^\alpha(\theta)$ is the critical resolved shear stress at current temperature, $\dot{\gamma}_0$ is a reference shearing rate and m is the rate sensitivity parameter.

The modified Voce-Kocks model is used to compute the slip system hardness,

$$\dot{\hat{\tau}}^\alpha = H_0 \left\{ \frac{\hat{\tau}_s(\dot{\gamma},\theta) - \hat{\tau}^\alpha(\theta)}{\hat{\tau}_s(\dot{\gamma},\theta) - \hat{\tau}_0} \right\} \dot{\gamma} \tag{10}$$

Where, H_0 is the initial work-hardening rate and $\hat{\tau}_0$ is the initial critical resolved shear stress. $\dot{\gamma}$ represents the sum of the shearing rate,

$$\dot{\gamma} = \sum_\alpha \dot{\gamma}^\alpha \tag{11}$$

The saturation value of hardness $\hat{\tau}_s$ is a function of the temperature and strain-rate based on the current slip system,

$$\hat{\tau}_s(\dot{\gamma},\theta) = \hat{\tau}_s^0(\frac{\dot{\gamma}}{\dot{\gamma}_s})^{m'} \tag{12}$$

Where, $\hat{\tau}_s^0$, $\dot{\gamma}_s$ and m' are the material constants.

In Taylor model, the macroscopic stress is obtained by averaging their respective values over all the grains. Assuming each crystal has the same volume, the macroscopic stress is computed by

$$\boldsymbol{\sigma}_{avg} = \frac{1}{N}\sum_{K=1}^{N}\boldsymbol{\sigma}_k \tag{13}$$

Where, N is the total number of crystals, $\boldsymbol{\sigma}_k$ is the Cauchy stress in the k th grain.

4. Integration algorithm

Firstly, the velocity gradient $\mathbf{L}$ and its thermal part $\mathbf{L}^{\boldsymbol{\theta}}$ representing deformation and thermal history are given. The total deformation gradient $\mathbf{F}_{t+\Delta t}$ at time $t+\Delta t$ can be computed by integrating $\mathbf{L}$ using the fourth Runge-Kutta algorithm. The task is to determine the stress, strain, hardness and orientation of a single crystal at time $t+\Delta t$.

The global velocity gradient is rotated to each material coordinate, and the stress associated with each grain is calculated relative to its own material coordinate. Then, local stress is rotated back to the global coordinate. Finally, the global stress is computed by Taylor model. The different computational progresses are introduced next.

4.1. summary of implicit algorithms

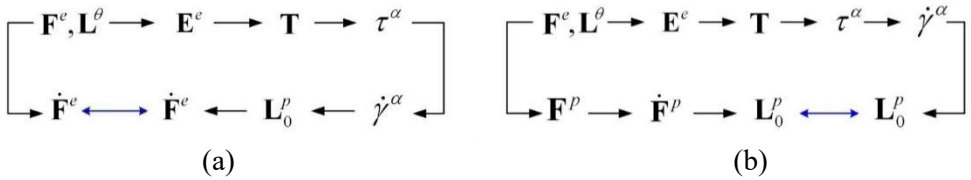

(a) (b)

Fig. 1 Computational process of implicit algorithms (a) $\mathbf{F}^e$ model (b) $\mathbf{F}^p$ model

Two implicit algorithms (elastic deformation gradient $\mathbf{F}^e$ and plastic deformation gradient as basic controlling variable) are summarized for computational process. In Fig.1(a), the computation of $\mathbf{F}^e$ algorithm started form the elastic deformation gradient $\mathbf{F}^e$ and the thermal part of velocity gradient $\mathbf{L}^\theta$, several intermediate variables are calculated and then equation of the variation of elastic deformation gradient can be deduced (clockwise). According to definition equation (4) , the changing rate of elastic deformation gradient can also be obtained (anticlockwise). Combined these two process, the evolution equation of elastic deformation gradient can be presented using back-Euler method, and the Newton-Raphson method is adopted to solve this governing equation. Similarly in Fig. 1(b), the governing equation of plastic deformation gradient $\mathbf{F}^p$ can be deduced using the different expressions of plastic velocity gradient $\mathbf{L}_0^p$. These two implicit algorithms have similar modeling approach, but the numerical implementation is different. The details of two implicit algorithms can be refer to literatures[12,14].

4.2. Explicit algorithm

In implicit algorithms, the Jacobian matrix should be updated in every iteration, and the formula deduction is complicated. In order to avoid those complex formula deduction, an explicit integration

algorithm based on an Euler forward scheme is presented, which the plastic deformation gradient is taken as the basic integration variable. The computational process is introduced next.

Given a deformation history and temperature history in the form of the velocity gradient $\mathbf{L}$ and thermal part of velocity gradient $\mathbf{L}^{\theta}$, algorithm begins with elastic deformation gradient at time t. The green strain and 2nd P-K stress can be computed as

$$\mathbf{F}^{e}(t)=\mathbf{F}(t)\mathbf{F}^{\theta^{-1}}(t)\mathbf{F}^{p^{-1}}(t) \tag{14}$$

$$\mathbf{E}(t)=\frac{1}{2}[\mathbf{F}^{e^{\mathrm{T}}}(t)\mathbf{F}^{e}(t)-\mathbf{I}] \tag{15}$$

$$\mathbf{T}(t)=\mathbf{C}(\theta):\mathbf{E}(t) \tag{16}$$

Then, the resolved shearing stress $\tau^{\alpha}(t)$ and the shearing rate $\dot{\gamma}^{\alpha}(t)$ are given by

$$\tau^{\alpha}(t)=\mathbf{F}^{e^{\mathrm{T}}}(t)\mathbf{F}^{e}(t)\mathbf{T}(t):\overline{\mathbf{P}}^{\alpha} \tag{17}$$

$$\dot{\gamma}^{\alpha}(t)=\dot{\gamma}_{0}\left|\frac{\tau^{\alpha}(\theta)}{\hat{\tau}^{\alpha}(\theta)}\right|^{\frac{1}{m}}sign(\tau^{\alpha}) \tag{18}$$

Considering plasticity incompressible condition $\det(\mathbf{F}^{p}(\tau))=1$, the plastic deformation gradient should be normalized. According to equation (6), $\mathbf{F}^{p^{-1}}(\tau)$ is obtained by

$$\mathbf{F}^{p^{-1}}(\tau)=\mathbf{F}^{p^{-1}}(t)[\mathbf{I}-\Delta t(\sum_{\alpha}\dot{\gamma}^{a}(t)\overline{\mathbf{P}}^{\alpha})] \tag{19}$$

The thermal part of velocity gradient is updated by equation (5). Next, the second P-K stress $\mathbf{T}(\tau)$ is computed by

$$\mathbf{F}^{e}(\tau)=\mathbf{F}(\tau)\mathbf{F}^{\theta^{-1}}(\tau)\mathbf{F}^{p^{-1}}(\tau) \tag{20}$$

$$\mathbf{E}(\tau)=\frac{1}{2}[\mathbf{F}^{e^{\mathrm{T}}}(\tau)\mathbf{F}^{e}(\tau)-\mathbf{I}] \tag{21}$$

$$\mathbf{T}(\tau)=\mathbf{C}(\theta):\mathbf{E}(\tau) \tag{22}$$

The critical resolved shear stress is updated by

$$\dot{\hat{\tau}}^{\alpha}(t)=H_{0}\left\{\frac{\hat{\tau}_{s}(\dot{\gamma},\theta)-\hat{\tau}^{\alpha}(\theta)}{\hat{\tau}_{s}(\dot{\gamma},\theta)-\hat{\tau}_{0}}\right\}\dot{\gamma}(t) \tag{23}$$

$$\hat{\tau}^{\alpha}(\tau)=\hat{\tau}^{\alpha}(t)+\Delta t\dot{\hat{\tau}}^{\alpha}(t) \tag{24}$$

The rotation of crystal is calculated via polar decomposition of elastic deformation gradient. Repeat the above process until the computation is done.

5. Numerical analysis

The anisotropic elasticity tensor for Al is determined using three independent elastic coefficients C_{11}, C_{12} and C_{44} in terms of temperature and the parameters for hardening model at three different temperatures are taken from the literature[14]. The computed stress-strain responses have been reported in literature[15], which will be introduced next.

For the plane strain compression deformation with thermal effects, the components of the velocity gradient are taken as $L_{11} = -L_{33} = 0.867$ and others are zeros. Deformation to a strain of 1.0 with certain temperatures was simulated using two different models. The time step of implicit model is $\Delta t = 0.0052$, and explicit model using time step is $\Delta t = 1.0 \times 10^{-5}$. Figure 2 shows the effective stress and effective strain relationships in isothermal conditions. It is seen that the yield stress and hardening ability drops with increasing temperatures, but the flowing stress getting status state quickly. The results are almost same, there is little deviation between curves under higher temperature.

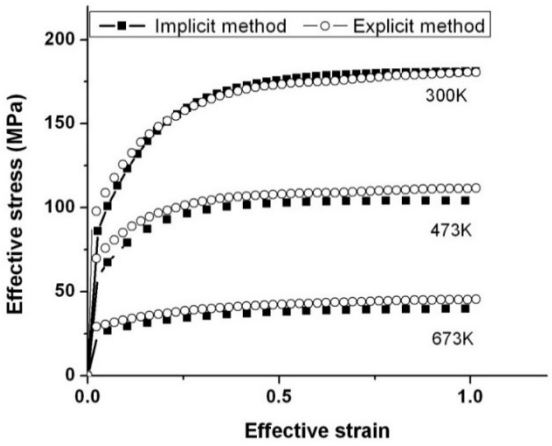

Fig. 2 The results of implicit algorithm and explicit algorithm under plane strain compression in different temperatures

In order to show the correctness of the model, a simple shear case was analysized where the velocity gradient components are taken as $L_{11} = L_{21} = L_{22} = 0$, $L_{12} = 2$. The $\mathbf{F}^p$ implicit model used to compute the effective strain and effective stress response at 300K. The results are compared with the report in Maniatty et al.[15], which is shown in Fig. 3. It can be seen that there is slightly decrease trend of stress when it reaches the maximum value, it could be caused by the changing of the slip systems numbers because of crystal rotation in the finite deformation.

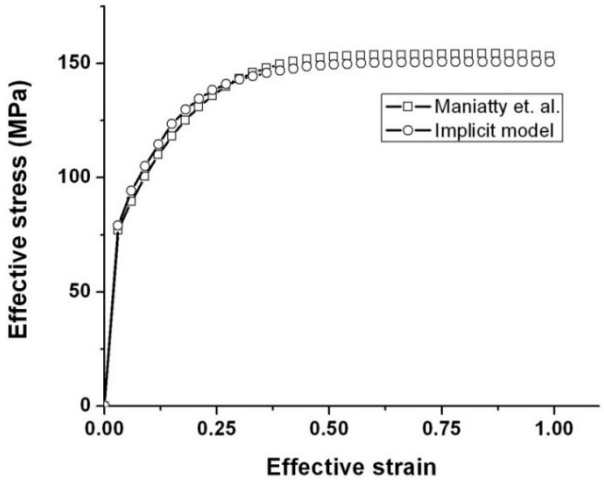

Fig. 3 The effective stress-effective strain curves for simple shear at 300K

In non-isothermal process, taking the plane strain compression as example, the $\mathbf{F}^e$ implicit model and explicit model were used to compute the effects of changing rates of temperature on the materials' mechanical behavior. Three different heating or cooling rates were considered, and the results are shown in Fig. 4. Fig. 4(a) shows the heating process. Softening phenomenon appears in the effective stress-effective strain curves, and this phenomenon is obvious at the high temperature with largest heating rate. Two algorithms of stress computation are basically the same, there is deviation of curves at high temperature. In cooling process, which can be seen form Fig. 4(b) that higher cooling rate resulting the stronger strengthen ability. Two algorithms of cooling process computation agree with each other.

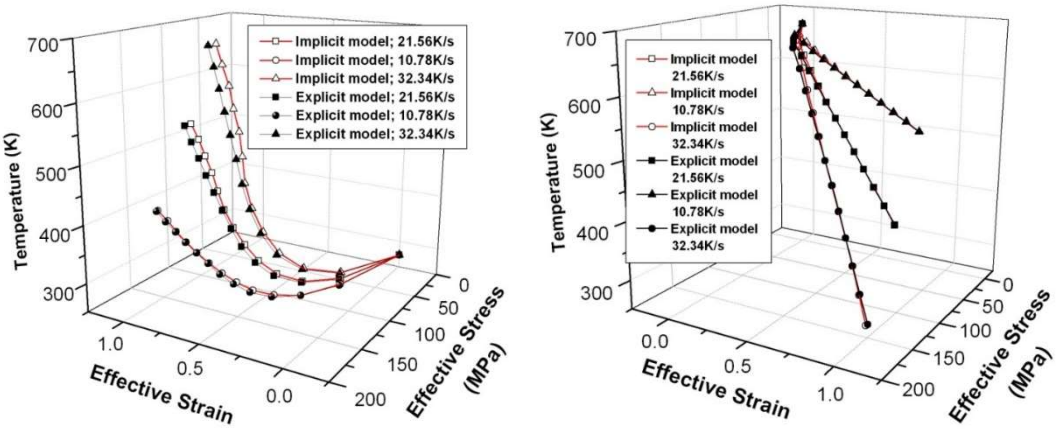

(a) (b)

Fig.4 The effect of temperature changing rates on effective stress-effective strain curve for plane strain compression comparing the results of implicit algorithm and explicit algorithm (a) different heating rates (b) different cooling rates

The effects of strain rate on materials' mechanical behavior in thermal process were also considered. $\mathbf{F}^e$ algorithm and explicit algorithm were computed in deformation of plane strain compression. The temperature changing rate is 21.56 K/s, and the strain rate range from $0.1s^{-1}$ to $10s^{-1}$. Figure 5(a) shows the effect of strain rates on effective stress-effective strain curve for plane strain compression comparing the results of implicit algorithm and explicit algorithm in heating process. It can be seen that the hardening is enhanced obviously as the strain rate increasing, the similar phenomena can be found in Li

et al.[16]. The cooling process shows in Figure 5(b). The results computed by two integration algorithms are almost same.

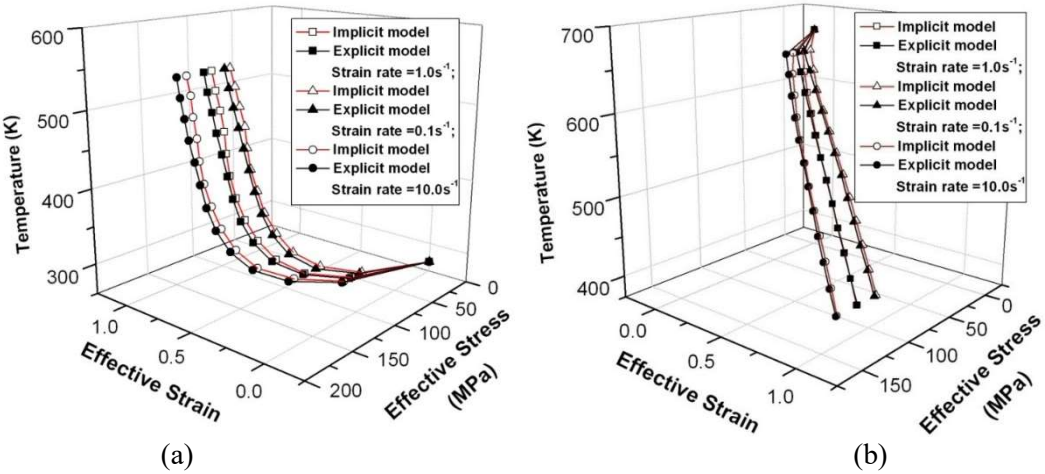

Fig. 5 The effect of strain rates on effective stress-effective strain curve for plane strain compression comparing the results of implicit algorithm and explicit algorithm (a) heating process (b) cooling process

It is observed that the material has positive strain-rate sensitivity in the thermal process, which means the flow stress and work hardening ability improve when the strain rate rises. But there are several aluminum alloys, for example AA 5182-O, display negative strain-rate sensitivity at room temperature. The flow stress and work hardening ability will decrease as the strain rate increases from 10^{-4} s^{-1}-1.0s^{-1}. Picu et al.[17] concluded that this phenomenon appearing due to the interaction of solute atoms with dislocations, and Khan et al.[18] also made the similar conclusions.

6. Conclusion

1. In this study, an explicit integration algorithm based on the forward Euler method for rate-dependent crystal plasticity with thermal effects was presented. The thermal effect can be described by the thermal velocity gradient, which contains the thermal history.

2. Several deformation patterns were analysized using these algorithms. The obtained effective stress and effective strain responses suggest that the explicit algorithm and the implicit algorithm has good stability. Finally, the effect of strain rate in thermal process was investigate and showed the positive strain-rate sensitivity in the thermal process.

Acknowledgments

This work was financially supported by the National Natural Science Foundation of China (No.11602158, No.11390362, No.51501123), the Natural Science Foundation for Young Scientists of Shanxi Province, China (Grant No.201601D021026) and the "1331 project" Key Innovation Teams of Shanxi Province, the Qualified Personnel Foundation of Taiyuan University of Technology (QPFT) (No.tyutrc-201439a). The financial contributions are gratefully acknowledged.

References

[1] G. R. Johnson, W. H. Cook, A constitutive model and data for metals subjected to large strains, high strain rates and high temperatures, (1983) 541-547.
[2] Ji Hyun Sung, Ji Hoon Kim, R. H. Wagoner, A plastic constitutive equation incorporating strain, strain-rate, and temperature, Int. J. Plasticity. 26 (2010) 1746-1771.
[3] A. Rusinek, J. A. Rodriguez-Martinez, A. Arias, A thermo-viscoplastic constitutive model for

FCC metals with application to OFHC copper, Int. J. Mech. Sci. 52 (2010) 120-135.
[4] Ming-Chun Cai, Li-Sha Niu, Xian-Feng Ma, Hui-Ji Shi, A constitutive description of the strain rate and temperature effects on the mechanical behavior of materials, Mech. Mater. 42 (2010) 774-781.
[5] Sangyul Ha, Jin-Hee Jang, KiTae Kim, Finite element implementation of dislocation-density-based crystal plasticity model and its application to pure aluminum crystalline materials, Int. J. Mech. Sci. 120 (2017) 249-262.
[6] Milan Ardeljan, Irene J. Beyerlein, Brandon A. McWilliams, Marko Knezevic, Strain rate and temperature sensitive multi-level crystal plasticity model for large plastic deformation behavior: Application to AZ31 magnesium alloy, Int. J. Plasticity. 83 (2016) 90-109.
[7] H. J. Frost, M. F. Ashby, Deformation mechanism maps: the plasticity and creep of metals and ceramics, (1982) 1-166.
[8] U. F. Kocks, A. S. Argon, M. F. Ashby, Thermodynamics and Kinetics of slip, Prog. Mater. Sci. 19 (1975) 1-127.
[9] S. Ganapathysubramanian, N. Zabaras, Modeling the thermoelastic-viscoplastic response of polycrystals using a continuum representation over the orientation space, Int. J. Plasticity. 21 (2005) 119-144.
[10] F. Roters, P. Eisenlohr, L. Hantcherli, D. D. Tjahjanto, T. R. Bieler, D. Raabe, Overview of constitutive laws, kinematics, homogenization and multiscale methods in crystal plasticity finite-element modeling: Theory, experiments, applications, Acta. Mater. 58 (2010) 1152-1211.
[11] Edward D. Cyr, Mohsen Mohammadi, Raja K. Mishra, Kaan Inal, A three dimensional (3D) thermo-elasto-viscoplastic constitutive model for FCC polycrystals, Int. J. Plasticity. 70 (2015) 166-190.
[12] D. Zhao, Y. G. Zhu, Y. Liang, P. Hu, Modeling and experimental verification of thermo-mechanical coupled behavior of face-centered-cubic polycrystals, Mater. Design. 52 (2013) 289-294.
[13] D. Peirce, C. F. Shih, A. Needleman, A tangent modulus method for rate independence solids, Computers and Structures. 18 (1984) 875-887.
[14] D. Zhao, Y. G. Zhu, P. Hu, W. X. Zhang, A new integration algorithm for thermo-elasto – viscoplastic single crystal finite deformation, Acta Mech. Sinica. 29 (2013) 709-717.
[15] A. M. Maniatty, P. R. Dawson, Y. S. Lee, A time integration algorithm for elasto-viscoplastic cubic crystals applied to modelling polycrystalline deformation, Int. J. Numer. Meth. Eng. 35 (1992) 1565-1588.
[16] D. Li, A. Ghosh, Tensile deformation behavior of aluminum alloys at warm forming temperatures, Mater. Sci. Eng. A 352 (2003) 279-286.
[17] R. C. Picu, G. Vincze, F. Ozturk, J. J. Gracio, F. Barlat, A. M. Maniatty, Strain rate sensitivity of the commercial aluminum alloy AA5182-O, Mater. Sci. Eng. A 390 (2005) 334-343.
[18] A. S. Khan, M. Baig, Anisotropic responses, constitutive modeling and the effects of strain-rate and temperature on the formability of an aluminum alloy, Int. J. Plasticity 27 (2011) 522-538.